Jens R. Stellhorn*, Shinya Hosokawa, Wolf-Christian Pilgrim, Yokinobu Kawakita, Kenji Kamimura, Koji Kimura, Nils Blanc, and Nathalie Boudet

Structural Aspects of the Superionic Conduction Mechanism in Ag-$GeSe_3$ Glasses

DOI 10.1515/zpch-2015-0667
Received July 27, 2015; accepted October 5, 2015

Abstract: The local and intermediate-range atomic structure in the Ag ion conducting glasses $Ag_x(GeSe_3)_{1-x}$ with $x = 0.15$ and 0.50 has been investigated by Anomalous X-Ray Scattering experiments at the K absorption edges of each constituent element. This method can provide insight into the structural properties enabling the effect of superionic conductivity for compositions with $x > 0.33$ in the amorphous phase. The experimental results were analyzed with Reverse Monte Carlo modeling, providing the partial structure factors and the corresponding partial pair-distribution functions. Evidence is found for a high level of intermediate range order for low silver concentrations, whereas the superionic conducting phase formed at high silver concentrations is characterized by cluster-like configurations of Ag atoms on a nanometer scale.

Keywords: Superionic Glass, Resonant X-ray Scattering, Synchrotron Radiation, Partial Structure, Intermediate-range, 3D Atomic Configurations.

***Corresponding author: Jens R. Stellhorn,** Department of Chemistry, Philipps-University of Marburg, Hans-Meerwein-Strasse 4, 35032 Marburg, Germany, e-mail: jens.stellhorn@chemie.uni-marburg.de
Shinya Hosokawa: Department of Physics, Graduate School of Science and Technology, Kumamoto University, Kumamoto 860-8555, Japan; and Department of Chemistry, Philipps-University of Marburg, Hans-Meerwein-Strasse 4, 35032 Marburg, Germany
Wolf-Christian Pilgrim: Department of Chemistry, Philipps-University of Marburg, Hans-Meerwein-Strasse 4, 35032 Marburg, Germany
Kenji Kamimura, Koji Kimura: Department of Physics, Graduate School of Science and Technology, Kumamoto University, Kumamoto 860-8555, Japan
Yokinobu Kawakita: J-PARC Center, Japan Atomic Energy Agency, Tokai 319-1195, Japan
Nils Blanc, Nathalie Boudet: Univ. Grenoble Alpes, Institut Néel and CNRS, Institut Néel, F-38000 Grenoble, France

1 Introduction

Superionic conducting materials are of growing interest in fundamental and applied materials' science, as they can e.g. be employed as electrolytes in solid-state batteries. Superionic glasses with a high ionic conductivity of $10^{-6}-10^{-2}$ S/cm are promising materials for such applications. It is well-known that superionic behavior in Ag containing chalcogenide glasses is observed at room temperature, such as for Ag-$GeSe_3$ alloys, in contrast to high temperatures needed in crystalline superionic conductors. Another advantage of these glasses as electrolytes is that the glassy state can easily be obtained in a wide concentration range by simple water or even air-quenching.

In the system $Ag_x(GeSe_3)_{1-x}$, a sharp jump of about eight orders of magnitude in the ionic conductivity is observed for $x > 0.33$ (corresponding to Ag concentrations of about 11 at %), where a superionic conducting phase is formed [1, 2]. The ionic conductivity of this phase is situated in the region $10^{-5}-10^{-4}$ S/cm. The exact position of the jump is somewhat controversial and has been reported with $x = 0.3$ [1] or $x = 0.26$ [2], determined by impedance measurements.

Based on thermodynamic data (i.e. glass transition and crystallization temperature measurements), Kawasaki et al. propose that three concentration regions should be differentiated: A region with low Ag concentrations and low conductivity between $0 \leq x \leq 0.2$, an intermediate region between $0.2 < x < 0.33$ and a region with high Ag concentrations and high ionic conductivity for $0.33 \leq x$. A large number of studies focuses on the structure of the superionic conducting phase: For a large range of Ag contents, the structural properties have been studied by Piarristeguy and coworkers by standard x-ray diffraction [3, 4] and neutron diffraction [5]. Ohara, Kumara and coworkers analyzed the structure by means of high-energy x-ray scattering, neutron diffraction, and EXAFS [6, 7], and most recently, our group discussed properties of the composition with $x = 0.50$ by anomalous x-ray scattering and reverse Monte Carlo (RMC) modeling [20]. All studies agree that the average coordination number of silver is remarkably high, with a value of 3 or more. Furthermore, chain-like fragments of Ag atoms can be clearly observed. But despite the large number of studies, a detailed analysis of the intermediate range order (IRO) of Ag-$GeSe_3$ glasses is still lacking. The IRO, such as the Ge-Se network in Ge_xSe_{1-x} glasses [8], is known to be a dominant feature in the structure of chalcogenide glassy systems. Yet it is difficult to resolve such structures by total scattering and/or EXAFS data alone, as pointed out e.g. by Waseda [9].

To achieve a more detailed insight into the structural basis of the superionic conduction threshold on the short- and intermediate length scale, we report here on anomalous x-ray scattering (AXS) experiments performed on $Ag_{0.15}(GeSe_3)_{0.85}$

and $Ag_{0.50}(GeSe_3)_{0.50}$ near x-ray energies close to the Ge, Se and Ag K-absorption edges, combined with Reverse Monte Carlo simulations (RMC). The atomic fractions of silver in these compounds are 4.2% and 20%, respectively. We will thereby discuss which structural properties distinguish the fast ion conducting phase from the insulating phase.

2 Principle of anomalous x-ray scattering

Anomalous x-ray scattering (AXS) utilizes the anomalous variation of the atomic form factor f of a specific element near an x-ray absorption edge, which is given as a function of energy E and momentum transfer Q:

$$f(Q,E) = f_0(Q) + f'(E) + if''(E), \tag{1}$$

where $f_0(Q)$ is the usual energy-independent term, and $f'(E)$ and $f''(E)$ are the real and imaginary parts of the anomalous term, respectively. In general, only when the incident x-ray energy approaches an absorption edge of a constituent element, the energy-dependent terms $f'(E)$ and $f''(E)$ become important. In fact, $f'(E)$ has a large negative minimum and $f''(E)$ shows an abrupt jump near the absorption edge energy. The resulting intensity contrast $\Delta_k I$ between two scattering functions (measured at energies E_1 and E_2, respectively) close to an absorption edge of element k can be expressed as

$$\Delta_k I(Q,E_1,E_2) \propto \Delta_k[\langle f^2\rangle - \langle f\rangle^2] + \Delta_k[\langle f\rangle^2]\Delta_k S(Q). \tag{2}$$

Here, $\Delta_k[\ ]$ indicates the difference of the values in the brackets at energies of E_1 and E_2. These values are chosen close to an absorption edge of the k-th element, typically some 100 eV and some 10 eV below the edge, respectively. The angular brackets denote the chemical average. Similar to a total scattering function $S(Q)$, these $\Delta_k S(Q)$ can be expressed by a linear combination of partial correlations $S_{ij}(Q)$ as

$$\Delta_k S(Q) = \sum_{i=1}^{N}\sum_{j=1}^{N} W_{ij}(Q,E_{\text{far}},E_{\text{near}})S_{ij}(Q), \tag{3}$$

with the weighting factors W_{ij}'s given as

$$W_{ij}(Q,E_{\text{far}},E_{\text{near}}) = x_i x_j \frac{\Delta_k[f_i f_j^*]}{\Delta_k[\langle f\rangle^2]}, \tag{4}$$

where x_i and f_i are the concentration and the atomic form factor of i-th element, respectively. Since the number of $S_{ij}(Q)$'s rises as $N(N+1)/2$, with N denoting

the number of elements, at least as many scattering experiments with different W_{ij}'s are, in principle, necessary to obtain a complete set of $S_{ij}(Q)$ for a multicomponent material.

Further details on the theoretical and experimental background of AXS can be found elsewhere [8–12].

3 Experimental procedure

3.1 Sample preparation

The amorphous samples of $Ag_x(GeSe_3)_{1-x}$ were prepared by water-quenching from the sealed mixture of the respective ratios of Ag, $GeSe_2$ and Se into a silica tube under vacuum. The resulting powder was pressed into a round pellet with a flat surface of about 13 mm in diameter. The concentrations and homogeneity were examined by x-ray diffraction and differential thermal analysis at several positions of the quenched samples.

3.2 AXS experiments

The AXS measurements were carried out in reflection geometry at the French CRG beamline BM02-D2AM of the European Synchrotron Radiation Facility (ESRF) in Grenoble, France. The diffraction experiments were performed on a standard ω-2θ diffractometer installed at the beamline using two incident x-ray energies (-20 or -30 eV, and -200 eV) below the K absorption edges of each constituent element. To obtain the $\Delta_k S(Q)$ in a high statistical quality, we used a bent graphite crystal energy-analyzer combined with a long (1 m) detector arm carrying a photomultiplier with a NaI scintillator to grant a good energy resolution capable to discriminate elastic signals from spurious inelastic contributions (i.e. resonant Raman signals and Compton scattering, cf. [13]) as well as a reasonable number of detected photons during the collection time. Details of the experimental setup are given elsewhere [11, 12].

The individual absorption edges were defined experimentally by fluorescence measurements. For the AXS data analysis, theoretical values for the term f_0 [14] were employed, as well as theoretical values for the anomalous terms f' and f'' tabulated by Sasaki [15]. The latter show a reasonable agreement to the experimental values for measurements not too close to the absorption edge (i.e. at energies some ten eV below the edge, see e.g. [13] for a comparison in the case of the

Table 1: Weighting factors W_{ij} of $S_{ij}(Q)$ for each dataset at $Q = 2.0\,\text{Å}^{-1}$ near the first peak position in $S(Q)$, for $x = 0.15$.

Dataset	AgAg	AgGe	AgSe	GeGe	GeSe	SeSe
$S(Q)$	0.003	0.024	0.077	0.051	0.326	0.518
$\Delta_{Ag}S(Q)$	0.051	0.228	0.723	0.001	0.001	−0.003
$\Delta_{Ge}S(Q)$	0.0001	0.058	0.008	0.181	0.677	0.077
$\Delta_{Se}S(Q)$	0.000	−0.001	0.070	−0.005	0.240	0.697

Table 2: Weighting factors W_{ij} of $S_{ij}(Q)$ for each dataset at $Q = 2.0\,\text{Å}^{-1}$ near the first peak position in $S(Q)$, for $x = 0.50$.

Dataset	AgAg	AgGe	AgSe	GeGe	GeSe	SeSe
$S(Q)$	0.059	0.088	0.280	0.033	0.209	0.331
$\Delta_{Ag}S(Q)$	0.234	0.184	0.582	0.000	0.000	0.000
$\Delta_{Ge}S(Q)$	0.003	0.251	0.034	0.138	0.516	0.058
$\Delta_{Se}S(Q)$	0.001	−0.005	0.298	−0.004	0.182	0.528

Se K-edge). Following a procedure outlined e.g. in [8, 10, 11], differential structure factors $\Delta_k S(Q)$ were calculated for each K edge.

As can be observed from the weighting factors $W_{ij}(Q)$, this method enhances the edge-related partial contributions $S_{ij}(Q)$ to $\Delta_k S(Q)$, and other partials are highly suppressed. This effect is particularly useful if the atomic fraction of an element is rather small, as e.g Ag in $Ag_{0.15}(GeSe_3)_{0.85}$. Exemplary, the W_{ij} values at 2 Å^{-1} near the structure factor maximum position are tabulated in Tables 1 and 2; the variation with Q is comparably small.

3.3 RMC modeling

In the RMC modelling procedure, the three differential structure factors for each element and one total structure factor obtained at an energy of 25.215 keV were included as experimental reference data. We employed the RMC_POT program package by Gereben et al. [16, 17]. We chose an input configuration with proper stoichiometry of 10 000 atoms for $x = 0.50 Ag_{0.50}(GeSe_3)_{0.50}$ and 24 000 atoms for $Ag_{0.15}(GeSe_3)_{0.85}$, randomly distributed in a cubic box corresponding to the number density of $\rho_{N,x=0.50} = 0.03758$ and $\rho_{N,x=0.15} = 0.03483$ atoms/Å^{-3} (cf. [3]), respectively. The higher number of atoms in the case $x = 0.15$ was chosen as to appropriately model the Ag based correlations, since the content of Ag atoms is

comparably small. Minimum atomic distances were defined in order to avoid unphysical configurations as 2.9, 3.1, 2.5, 3.1, 2.1, and 2.1 Å for the Ag-Ag, Ag-Ge, Ag-Se, Ge-Ge, Ge-Se, and Se-Se distance, respectively. The values for the Ge-Ge and Ag-Ge distances were chosen so that these bonds do not contribute to the first coordination shell, marked by the minimum in the total pair correlation function $g(r)$ at 3.0 Å, because the existence of such bonds has been disproved by EXAFS measurements [7]. Both values were increased for $x = 0.50$ to 3.3 Å in order to appropriately model the second coordination shell. After confirming a coordination number of about 4 for the Ge-Se bond in each simulation, a weak bond angle constraint has been applied subsequently to ensure a tetrahedral bonding coordination of Se around Ge atoms. For $x = 0.15$, the number of Se-Se bonds was found considerably higher than in comparable experiments (cf. Table 3) in the first simulation run, so that a Se-Se coordination number constraint was applied.

4 Results and discussion

Experimental data and RMC fits. The total and differential structure factors calculated from the experimental data together with the best fits obtained from the RMC simulation are displayed in Figure 1. The total structure factors obtained in the AXS experiments agree well with the $S(Q)$ data from other diffraction experiments [4, 18]. In all Ag-$GeSe_3$ compositions in [4], a small first sharp diffraction peak (FSDP) can be seen in the low-Q region at $Q_1 \approx 1.05$ Å^{-1}. The intensity of this peak decreases steadily as a function of the Ag content x [4]. There are two peaks of nearly similar intensity located at $Q_2 = 2.0$ Å^{-1} and $Q_3 = 3.4$ Å^{-1}. The last comparably pronounced peak is situated broadly around $Q_4 = 5.45$ Å^{-1}.

The differential structure factors $\Delta_k S(Q)$ coincide in their general form in both glasses. However, an important difference is the FSDP in $\Delta_{Ag} S(Q)$, which is quite pronounced in $x = 0.15$, but missing in $x = 0.50$. It is noteworthy that the decrease in intensity of the FSDP as a function of x is well known in the literature only regarding the total structure factor (e.g. [3, 4]). On the other hand, our AXS experiments show that the FSDP of the $\Delta_{Ge} S(Q)$ and $\Delta_{Se} S(Q)$ functions remains generally unchanged, and only the FSDP in the Ag related functions decreases with x. In turn, this development leads to the reduction of the FSDP in the total structure factor.

The features of the $\Delta_{Se} S(Q)$ and the $\Delta_{Ge} S(Q)$ closely resemble the corresponding functions in pure $GeSe_3$ [8], except that the FSDP in the $\Delta_{Se} S(Q)$ of $GeSe_3$ is only visible as a small shoulder of the first structure factor peak. In the two Ag-$GeSe_3$ glasses under consideration, only slight differences are observed

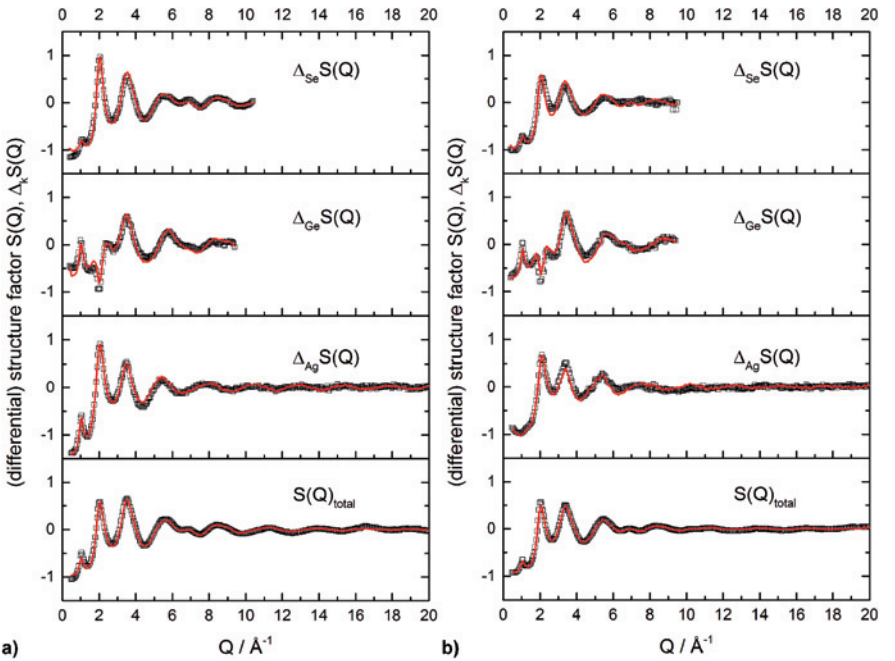

Figure 1: Experimentally determined total structure factor $S(Q) - 1$ at 25.214 keV and $\Delta_k S(Q) - 1$ around the Ag, Ge and Se K edges, for $x = 0.15$ (a) and $x = 0.50$ (b). Squares indicate data obtained from the AXS experiments, and solid curves denote the best fits by RMC modeling.

for the two compositions, i.e. compared with $Ag_{0.50}(GeSe_3)_{0.50}$, the minimum in $\Delta_{Ge}S(Q)$ at the Q_2 position is more pronounced for $Ag_{0.15}(GeSe_3)_{0.85}$, and the peaks at Q_2 and Q_3 in $\Delta_{Se}S(Q)$ are more intense.

Partial structure factors. The partial structure factors obtained from the RMC modelling procedure are displayed in Figure 2 (the corresponding pair distribution functions are shown in Figure 3). The general form of the Se-Se and Ge-Se correlation coincides well for both compositions, indicating that the corresponding partial structural motives do not change considerably. The most notable contrast is that the signals at the Q_2 position (i.e. the peak in Se-Se and the dip in Ge-Se) are more pronounced in $x = 0.50$. The other $S_{ij}(Q)$'s, on the other hand, exhibit major differences: The peaks in the Ge-Ge, Ag-Ge and Ag-Ag correlations at the Q_2 position become much narrower in $x = 0.50$, and the Ag-Ag correlation also displays a more intense signal in the low-Q region. And whereas the Ag-Se correlation is very similar to the total $S(Q)$ in $x = 0.15$, it exhibits a minimum at the Q_2 position in $x = 0.50$.

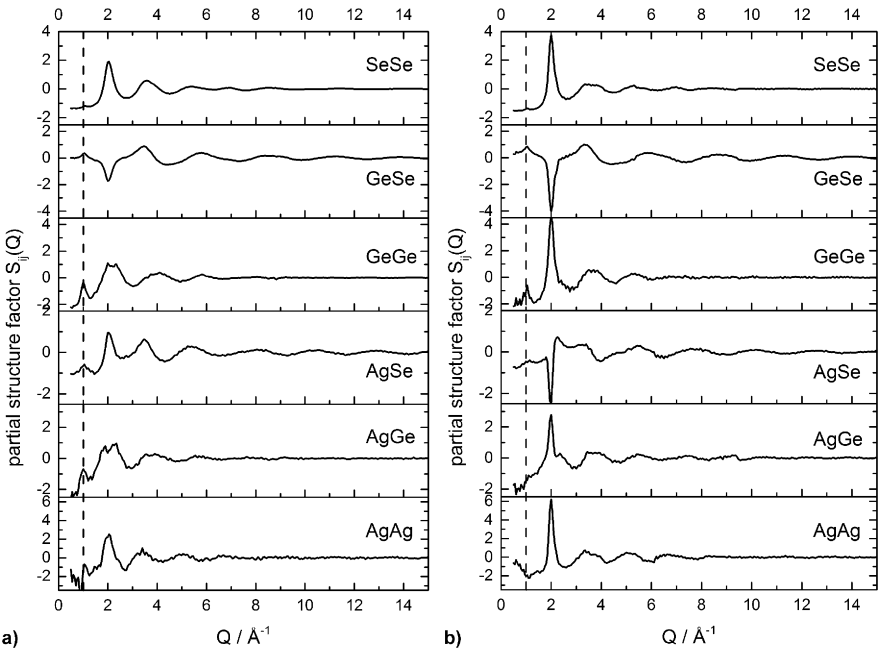

Figure 2: Partial structure factors $S_{ij}(Q) - 1$ obtained by RMC, for $x = 0.15$ (a) and $x = 0.50$ (b). The dashed line at $Q = 1$ Å^{-1} is a guide for the eye.

The most striking difference, however, is the behaviour of the FSDP. Below the superionic conductivity threshold at about 11 at %, the FSDP is visible in every $S_{ij}(Q)$, though only with a small intensity in the Se-Se correlation. Such FSDP's are absent in all Ag based correlations for $x = 0.50$, but they can be observed in the Se-Se, Ge-Se and Ge-Ge correlations, though they are less pronounced compared to those for $x = 0.15$. This indicates a high degree of intermediate range order in the low ionic conducting phase.

In $GeSe_3$, the FSDP was found to be majorly attributed to the Ge-Se and Ge-Ge correlations and has been considered to represent chains of $GeSe_4$ tetrahedra, which form a glassy network structure on the intermediate length level [4, 8]. Such a network, interspersed with Ag atoms, is also observed in the configurations obtained by RMC in the Ag-$GeSe_3$ glasses, as illustrated in Figure 4. Piarristeguy et al. [4] interpreted the decrease of the FSDP in the total $S(Q)$ as a fragmentation of the $GeSe_4$ tetrahedra chains with rising content of Ag, based on the assumption that the FSDP is majorly related to the Ge-Ge correlation of neighbouring tetrahedra. The AXS/RMC results presented here indeed reveal a slight reduction in the Ge-Ge related FSDP. However, it should be emphasized that the Ge-Ge correla-

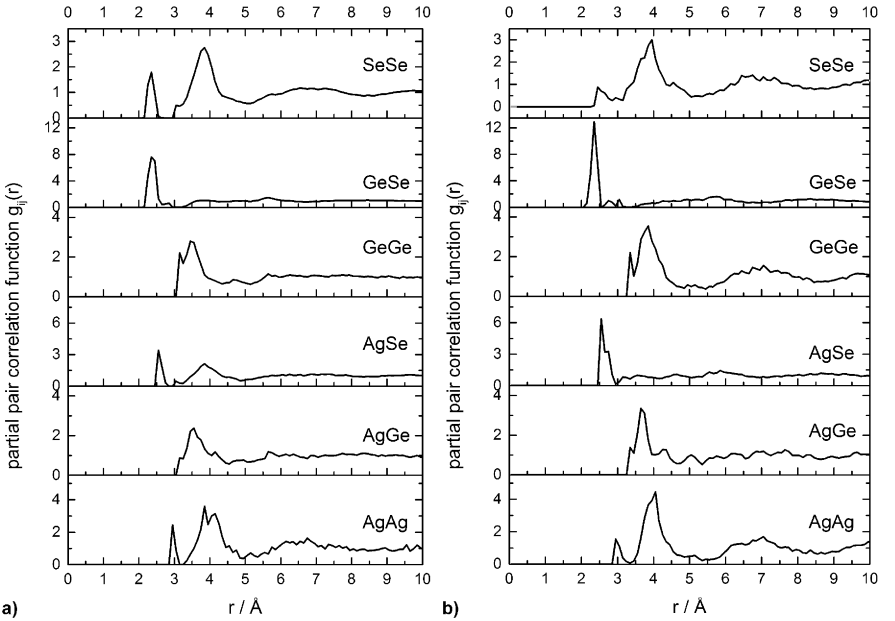

Figure 3: Partial pair correlation functions $g_{ij}(r)$ obtained by RMC, for $x = 0.15$ (a) and $x = 0.50$ (b).

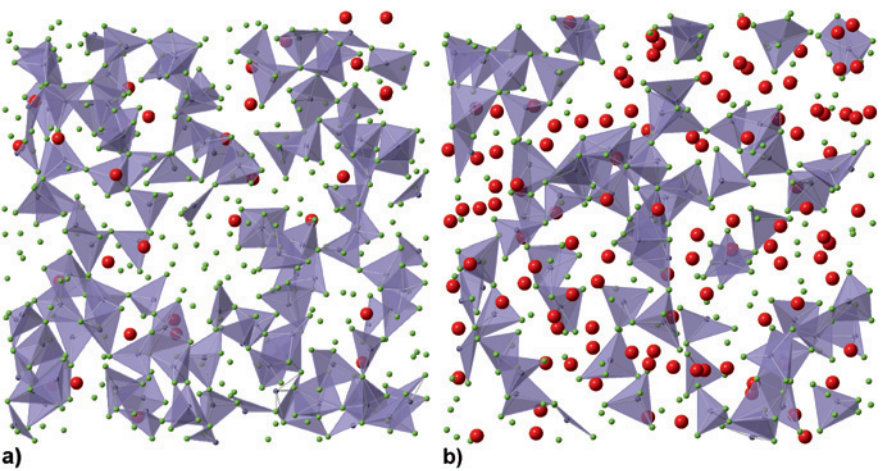

Figure 4: 32×32 Å^2 section of the configuration of $x = 0.15$ (a) and $x = 0.50$ (b) obtained by RMC, showing Ge-Se coordination polyhedra (red: Ag, green: Se, blue: Ge).

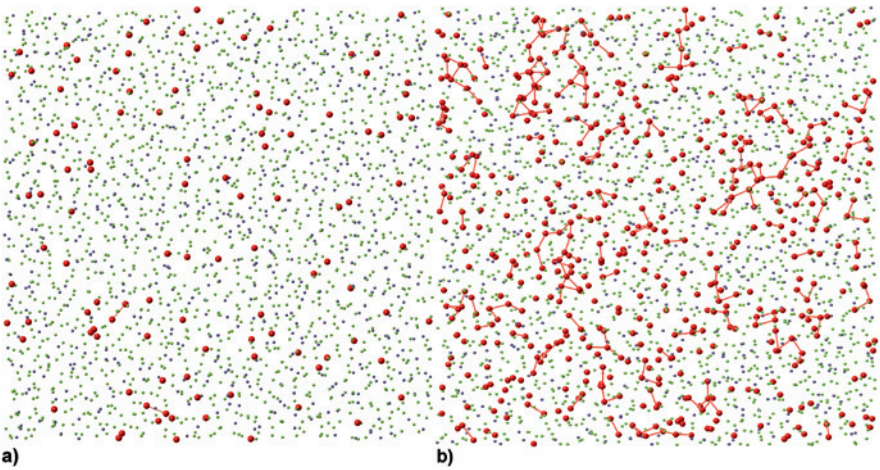

Figure 5: $64 \times 64 \times 13$ Å^3 sections of the configuration of $x = 0.15$ (a) and $x = 0.50$ (b) obtained by RMC. The latter shows distinct regions with high or low density of Ag atoms, respectively (red: Ag, green: Se, blue: Ge).

tion is not the major reason for the decrease of the FSDP in the total $S(Q)$. This effect is rather constituted by the reduction of the FSDP's in the Ag-based correlations. We may also point out that a reduction of the FSDP upon addition of Ag is also observed in comparable systems, like germanium-sulfide glasses of similar composition (i.e. the Ag-GeS_3 system) [26].

Furthermore, the signal in the low Q-region of $S_{\mathrm{AgAg}}(Q)$ in $x = 0.50$ can be interpreted as a sign for an emerging phase separation tendency, which has been point of some debate in the superionic conducting phase [7]. This tendency is illustrated in Figure 5, where regions of high concentrations of Ag atoms (shown in red) are clearly bordered by regions of low Ag concentration against a background of Se (green) and Ge (blue). In contrast, the Ag atoms in $x = 0.15$ are found to be statistically distributed among the other atoms.

Partial pair correlation functions and SRO. The partial pair correlation functions $g_{ij}(r)$ obtained by RMC are displayed in Figure 3. Two coordination shells can be clearly distinguished: the first extends to about 3 Å (or 3.3 Å for the Ag-Ag correlation), and the second extends to about 4.5 Å, with maxima between 3.5 and 4.0 Å. Major differences in the $g_{ij}(r)$'s are observed in the homopolar Se-Se and Ag-Ag correlations: Firstly, $g_{\mathrm{SeSe}}(r)$ in $x = 0.15$ exhibits a sharp first coordination sphere around 2.4 Å, whereas the peak decreases in intensity and is partly superimposed by the second coordination sphere centered at 3.85 Å in $x = 0.50$. Secondly, the coordination number for the Ag-Ag correlation considerably increases

Table 3: Partial and total coordination numbers of the first and second coordination shell obtained by AXS/RMC in comparison with other studies (see text). Coordination numbers have been calculated by integrating the respective coordination shells in the $g_{ij}(r)$ up to 3 and 4.5 Å, respectively (3.3 Å in case of the first CN of Ag-Ag).

	low conductivity			high conductvity		
	AXS [8]	this work	Mo-K_α [3, 4]	this work	Mo-K_α [3, 4]	EXAFS [7]
x	0	15	30.7	50	50	56.5
at %Ag	0	4.2	10	20	20	24.5
AgAg		0.08	0.20	0.45	0.60	0.60
AgGe		0.00	0.45	0.00	0.60	
AgSe		2.17	1.35	2.80	1.80	2.20
GeAg		0.00	0.20	0.00	0.60	
GeSe	4.00	4.07	3.91	3.98	3.90	3.70
SeAg		0.13	0.20	0.93	0.60	0.90
SeGe	1.33	1.36	1.30	1.33	1.30	1.20
SeSe	0.67	0.78	0.61	0.65	0.60	N/A
$AgAg_{2nd}$		0.7		3.6		
$AgGe_{2nd}$		2.9		2.6		
$AgSe_{2nd}$		8.5		(4.6)		
$GeGe_{2nd}$		3.2		3.5		
$SeSe_{2nd}$		10.5	11.0	9.2	10.7	
N(Ag)		2.25	2.00	3.25	3.00	2.80
N(Ge)	4.00	4.07	4.11	3.98	4.50	3.70
N(Se)	2.00	2.26	2.11	2.91	2.50	N/A
$\langle N \rangle$	2.50	2.70	2.56	3.19	3.00	

from 0.08 to 0.45, with the peak centered near 3 Å. Note that this gain in the coordination number is related to the different concentration of Ag rather than the form of the $g_{\mathrm{AgAg}}(r)$'s. Both compositions exhibit a distinct signal at 2.35 Å in the Ge-Se correlation with a coordination number of $n_{\mathrm{Ge-Se}} \approx 4$, indicating the tetrahedral coordination of Se around Ge atoms. Indeed, four-fold coordinated Ge atoms represent the dominant structural feature: in $x = 0.15$ about 65% of all Ge atoms belong to this class, another 18% are five-fold coordinated. Comparable values are found in $x = 0.50$, where 68% of the Ge atoms are four-fold and 21% are five-fold coordinated. Also observed in both compositions are peaks at 2.6 Å in the Ag-Se correlation, though they are broadened in $x = 0.50$. Due to the applied constraints, Ge-Ge and Ag-Ge correlations only contribute to the second coordination sphere.

Table 4: Interatomic distances in Å obtained by AXS/RMC in comparison with other experiments.

	low conductivity			high conductvity		
	AXS [8]	this work	Mo-K_α [3, 4]	this work	Mo-K_α [3, 4]	EXAFS [7]
x	0	15	30.7	50	50	56.5
at %Ag	0	4.2	9.7	20	20	24.5
AgAg		2.95	3.05	2.95	3.05	2.8–2.9
AgGe						
AgSe		2.6	2.67	2.6	2.67	2.6
GeSe	2.35	2.35	2.37	2.35	2.39	2.34
SeSe	2.2	2.35	2.37	2.45	2.39	2.5
$AgAg_{2nd}$		3.9		3.9		3.6
$AgGe_{2nd}$		3.55		3.65		
$AgSe_{2nd}$		–		3.9		
$GeGe_{2nd}$	3.4	3.45		3.85		3.8
$SeSe_{2nd}$	3.9	3.85	3.85	3.85	3.88	

A complete overview of all coordination numbers and interatomic distances extracted from the $g_{ij}(r)$'s is given in Tables 3 and 4. The results are compared with other experimental data as follows:

1) For the low conducting phase ($x = 0.15$), the data are compared with AXS experiments of the pure $GeSe_3$ [8] and with a total scattering experiment on a composition with 10 at % Ag (i.e. $x = 30.7$ [4]).

2) For the superionic conducting phase ($x = 0.50$), a total scattering experiment on $x = 0.50$ [3, 4] and an EXAFS/RMC experiment on the composition $x = 0.565$ [7] are taken as comparison.

It should be noted that though the focus of the study in [3, 4] is on the superionic conducting phase, it can be questioned whether the composition denoted $(Ge_{0.25}Se_{0.75})_{90}Ag_{10}$ (i.e. $x = 0.31$) is definitely part of this phase. According to [1], this composition would be situated in the intermediate phase between $0.2 < x < 0.33$. Though it is not explicitly discussed in [4], a transition of short-range order (SRO) parameters is observed between the compositions containing corresponding to $x = 0.31$ and compositions $x = 0.41$, mainly related to the Ag coordination which changes from 2 to 3. Due to a reasonable agreement with the parameters obtained for AXS on $x = 0.15$, we will assume in the following that the respective data in [4] refer to an insulating phase.

It is interesting at this point to compare again the change in the short range order of the Ag-$GeSe_3$ glasses with the trends observed in the corresponding sulfide glasses Ag-GeS_3 [26]. In the pure GeS_3 glass, sulfur is two-fold coordinated, whereas the total coordination number rises as a function of the Ag content and

reaches 3 for $x = 0.50$. The total coordination number of Ag rises as well, but is already as high as 2.9 at low concentrations of Ag [26].

In general, coordination numbers and distances in Tables 3 and 4 are in good agreement with reference data. Coordination numbers obtained from EXAFS appear to be somewhat underestimated. It should also be taken into account that the total scattering experiments provide only a comparably low information content, thus explaining some differences in the obtained coordination numbers. However, total coordination numbers around each element taken from [3, 4] are in good agreement with the AXS results presented here, except for Ge in $x = 0.50$, for which Piarristeguy et al. propose a coordination number of 4.5. Such a high coordination is very unusual for Ge and indeed, this value also contradicts findings from EXAFS experiments [7].

Intermediate range order. The Se-Se bond distance of about 3.85 Å is usually interpreted as the Se-(Ge)-Se distance inside the $GeSe_4$ tetrahedra [8, 18]. The coordination number of this second neigbour Se-Se correlation decreases from 10.5 for $x = 0.15$ to 9.2 for $x = 0.50$, exhibiting the same trend as in [3]. The differences to the values in [3] may also result from the difficulty to unambiguously define the borders of the second coordination sphere. The coordination number of the second coordination shell of the Ge-Ge correlation remains nearly constant, but the interatomic distance increases from 3.45 to 3.85 Å. The bond distance of about 3.4 Å agrees well with the value found for the corner-sharing configuration of $GeSe_4$ tetrahedra in Ge_ySe_{100-y} glasses [4, 21]. In this respect, the coordination number of the second neighbour Ge-Ge correlation can be interpreted as a measure for the strength of the $GeSe_4$ tetrahedral network, indicating the strong connectivity in both the materials. The elongation of the Ge-Ge distance is also accompanied by a shift of the maximum in the Ge-Se-Ge bond angle distribution from 90° to nearly 109°, as illustrated in Figure 6. A 90° Ge-Se-Ge bond angle is the result of bonding via the *p*-orbitals of Se, with a lone electron pair in the remaining *p*-orbital. This is the case in $x = 0.15$, exhibiting a total coordination number $N_{Se} = 2.26$. For $x = 0.50$, however, N_{Se} rises to 2.91, mainly due to an increased number of Se-Ag bonds. The interaction of the Ag atom with the lone pair at Se thus causes the Ge-Se-Ge bond angle to increase. This effect is important to understand the nature of the tetrahedral network and schematically depicted in Figure 7. In addition, it is found that these Ag-Se bonds are formed at the expense of the second coordination shell at 3.9 Å, which is clearly developed only in $x = 0.15$; this is reflected not only in the $g_{AgSe}(r)$, but also in the Se-Se-Ag bond angle distribution in Figure 6, which shows a distinct bond angle distribution around 105° only for $x = 0.15$. This correlation thereby illustrates the principal contribution to the loss of IRO in the Ag based correlations in $x = 0.50$.

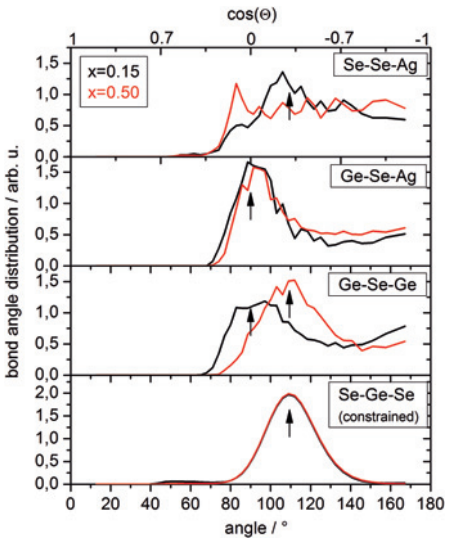

Figure 6: Bond angle distributions of Se-Ge-Se, Ge-Se-Ge, Ge-Se-Ag and Se-Se-Ag (from bottom to top) in $x = 0.15$ (black) and $x = 0.50$ (red). Arrows indicate angles of 109.5° and 90°, respectively.

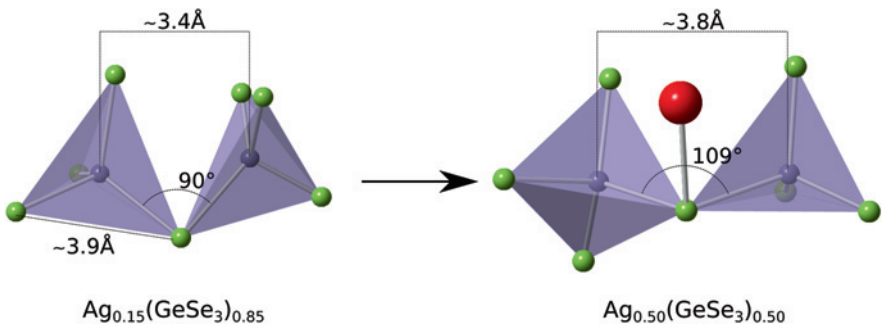

Figure 7: Schematic view of the expansion in the $GeSe_4$ network upon increase of Ag content x (red: Ag, green: Se, blue: Ge).

The final structural aspect to be discussed is the Ag-Ag correlation. As seen in Figure 3, the partial pair correlations $g_{AgAg}(r)$ in both glasses are surprisingly similar at first glance. The first and second coordination shells increase proportional to the Ag concentration in terms of the coordination number, and also the interatomic distances remain the same. However, as illustrated in Figure 5, there are major differences in the distribution of the Ag atoms over the simulation box. $Ag_{0.50}(GeSe_3)_{0.50}$ tends to form cluster-like configurations of Ag atoms on a nanometer length scale, whereas in $Ag_{0.15}(GeSe_3)_{0.85}$, the Ag atoms tend to distribute randomly over the whole considered volume. A closer inspection can be achieved by a statistical analysis as shown in Figure 8, which displays the prob-

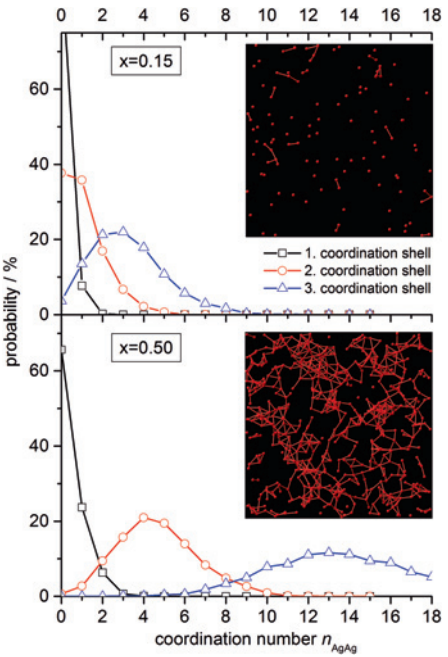

Figure 8: Probability of finding an Ag ion with the indicated number of neighbouring Ag ions in the respective coordination shells. The insets illustrate the Ag distribution in a 64×64 Å^2 section on the level of the second coordination shell.

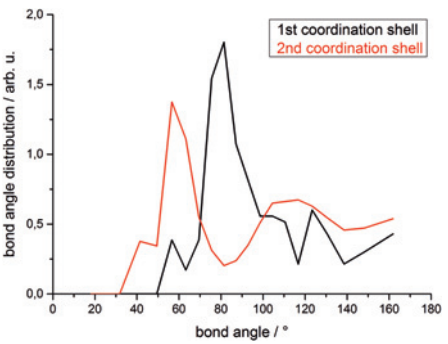

Figure 9: Bond angles of Ag-Ag-Ag chains on the level of the first and second coordination shell.

ability of finding an Ag ion with the indicated number of neighbouring Ag ions. The distributions are separately shown for the first, second and third coordination shells, respectively. It is found that on the next neighbour scale, the majority of Ag atoms do not form homopolar bonds, and only 7.1 % are two-fold coordinated, and may thus be the basis for chains of Ag atoms in the composition with $x = 0.50$. On the other hand, the Ag atoms form a pronounced network with distinct vacancies on the intermediate length level. The insets in Figure 8 illustrate the Ag network on the level of the second neighbors. A similar finding was reported by Ohara and coworkers [6]. This intermediate network is characterized by bond angles of 60°

and a broad distribution around 110°, as displayed in Figure 9, majorly differing from the bond angles observed on the next neighbour level, possessing a peak around 80°.

Impact on the ion conduction mechanism. The data presented here permit the discussion of the structural changes enabling the superionic conductivity in Ag-$GeSe_3$ glasses. A substantial change in the short-range order is observed upon increasing the Ag content above the superionic conductivity threshold at $x = 0.33$. The superionic phase is characterized by high average coordination numbers around selenium and silver. The network of corner-shared $GeSe_4$ tetrahedra widens due to the Ag-Se interaction, as indicated by the Ge-Se-Ge bond angle distribution and Ge-Ge distances, while the tetrahedra connection remains similarly strong. The expanded network incorporates the higher number of Ag atoms, which form small cluster-like configurations on the nanometer length scale in which Ag-Ag homopolar bonds are concentrated. These clusters lead to the loss of intermediate range order of the Ag atoms as represented by the decrease of the Ag-related FSDPs. Equivalently, regions of high and low Ag concentrations are formed, which act as conduction pathways for the Ag atoms.

However, from the present data it cannot yet be concluded whether the jump in ionic conductivity is associated with a comparably sharp change in the glass structure, or whether the structural changes are a continuous function of x. Since it is reported that even within one phase (i.e. the fast ionic conducting phase), short-range order parameters can change significantly as a function of the Ag content [4], we are currently performing further investigations near the superionic conductivity threshold in order to study the nature of the jump in ionic conductivity.

The authors are aware that ternary $Ag_x(Ge_ySe_{1-y})_{1-x}$ glasses have been reported to be macroscopically phase separated on the entire concentration range of Ag under investigation. This finding is based on glass transition temperature measurements (DSC) [22], scanning electron microscopy (SEM) [23] and electric force microscopy (EFM) [24, 25]. The investigations agree in so far as they report a transition from an Ag-rich phase immersed in a Ge-Se phase for low Ag concentrations to a structure with Ag-poor zones immersed in an Ag-rich network. The size of the respective regions, however, appears to be a point of discussion: For the insulating phase (< 10 at % Ag), the size of the Ag-rich inclusions have been reported to be 1–3 μm [22], 1 μm [24] or 110 nm [23]. The Ag-poor inclusions observed for the phase with 20 at % Ag are reported to be 250–500 nm [24] or 700 nm [23]. The authors of the latter article also report that the composition with 25 at % Ag is nearly homogeneous.

Inhomogeneities probed by electron microscopy naturally describe only the surface of the samples, which may differ considerably from the bulk structure. The DSC measurements indicate a phase separation in the bulk material, but can provide no details on the size of the separated volumes. The AXS results of the present study, in contrast, can only give an average structure of the material and provide no information about a macroscopic phase separation. On the other hand, an onset of the separation of Ag-rich and Ag-poor phases is observed in the present AXS study, albeit on the nanometer range. Further insight into such structural details can be obtained by small angle scattering data, which we plan to gather in a subsequent series of experiments.

5 Summary

We performed an anomalous x-ray scattering experiment on the Ag ionic conducting glasses $Ag_{0.15}(GeSe_3)_{0.85}$ and $Ag_{0.50}(GeSe_3)_{0.50}$. By RMC modelling, the real-space model configurations were created which are in agreement with the total and differential structure factors obtained in the experiment. These configurations directly provide information on the partial functions $S_{ij}(Q)$ and $g_{ij}(r)$. Based on the RMC results, the structural prerequisites for the effect of superionic conductivity for $x = 0.50$ are discussed. In agreement with other studies, we find a substantial difference in the short-range below and above the superionic conductivity threshold of $x = 0.33$, in particular that the superionic phase is characterized by high average coordination numbers around Se and Ag.

It was confirmed that the Ag-Se interaction expands the $GeSe_4$ tetrahedral network, which constitutes a dominant structural feature in both glasses. Inside the expanded network, Ag atoms form cluster-like configurations on an intermediate length level, thereby destroying the IRO in the Ag based correlations in the fast ionic conducting phase. This development is manifested in the reduction of the FSDP of the total structure factor. Further AXS experiments are planned on $Ag_x(GeSe_3)_{1-x}$ glasses, with x close to the superionic threshold composition, in order to study the nature of the sharp jump in the ionic conductivity.

Acknowledgement: The AXS experiments were performed in collaboration with Dr. J.-F. Bérar at BM02/ESRF (Exp. Nos. HD 540 and HC1137). Supporting AXS experiments were performed at BL13XU/SPring-8 (Proposal No. 2014A1060). This work was partially supported by JSPS Grant-in-Aid for Scientific Research on Innovative Areas '3D Active-Site Science' (No. 26105006).

References

1. M. Kawasaki, J. Kawamura, Y. Nakamura, and M. Aniya, Solid State Ionics **123** (1999) 259.
2. A. Piarristeguy, J. M. Conde Garrido, M. A. Ureña, M. Fontana, and B. Arcondo, J. Non-Cryst. Solids **353** (2007) 3314.
3. A. Piarristeguy, M. Mirandou, M. Fontana, and B. Arcondo, J. Non-Cryst. Solids **273** (2000) 30.
4. A. Piarristeguy, M. Fontana, and B. Arcondo, J. Non-Cryst. Solids **332** (2003) 1.
5. G. J. Cuello, A. Piarristeguy, A. Fernández-Martínez, M. Fontana, and A. Pradel, J. Non-Cryst. Solids **353** (2007) 729.
6. K. Ohara, L. S. R. Kumara, Y. Kawakita, S. Kohara, M. Hidaka, and S. Takeda, J. Phys. Soc. Jpn. **79** (2010) Suppl. A 141.
7. L. S. R. Kumara, K. Ohara, Y. Kawakita, S. Kohara, P. Jóvári, M. Hidaka, N. E. Sung, B. Beuneu, and S. Takeda, Eur. Phys. J. Web Conf. LAM14 (2011) 02007-1-5.
8. S. Hosokawa, I. Oh, M. Sakurai, W.-C. Pilgrim, N. Boudet, J.-F. Bérar, and S. Kohara, Phys. Rev. B **84** (2011) 014201.
9. Y. Waseda, *Novel Application of Anomalous X-ray Scattering for Structural Characterization of Disordered Materials*, Springer-Verlag, Heidelberg (1984).
10. J. R. Stellhorn, S. Hosokawa, and W.-C. Pilgrim, Z. Phys. Chem. **228** (2014) 1005.
11. S. Hosokawa, Y. Wang, J.-F. Bérar, J. Greif, W.-C. Pilgrim, and K. Murase, Z. Phys. Chem. **216** (2002) 1219.
12. S. Hosokawa, W.-C. Pilgrim, J.-F. Bérar, and S. Kohara, Eur. Phys. J. Special Topics **208** (2012) 291.
13. H. E Fischer, A. C. Barnes, and P. S. Salmon, Rep. Prog. Phys. **69** (2006) 233.
14. C. H. MacGillavry and G. D. Rieck (Eds.), *International Tables for X-ray Crystallography*, 2nd edn., Vol. III Kynoch, Birmingham (1968).
15. S. Sasaki, *KEK Report 1989*, Nat. Lab. High Energy Phys., Tsukuba (1989), p. 1.
16. R. L. McGreevy and L. Pusztai, Mol. Simulat. **1** (1988) 359.
17. O. Gereben, P. Jóvári, L. Temleitner, and L. Pusztai, J. Optoelectron. Adv. M. **9** (2007) 3021.
18. R. Suenaga, Y. Kawakita, S. Nakashima, S. Tahara, S. Kohara, and S. Takeda, J. Phys. Conf. Ser. **98** (2008) 012021.
19. S. Sato and K. Maruyama, J. Phys.-Condens. Mat. **25** (2013) 454208.
20. J. R. Stellhorn, S. Hosokawa, Y. Kawakita, D. Gies, W.-C. Pilgrim, K. Hayashi, K. Ohoyama, N. Blanc, and N. Boudet, J. Non-Cryst. Solids (2015) DOI:10.1016/j.jnoncrysol.2015.02.027.
21. P. Armand, A. Ibanez, H. Dexpert, D. Bittencourt, D. Raoux, and E. Philippot, J. Phys. IV Colloque C2 (2) (1992) C2-189.
22. Y. Wang, M. Mitkova, D. G. Georgiev, S. Mamedov, and P. Boolchand, J. Phys.-Condens. Mat. **15** (2003) S1573.
23. B. Arcondo, M. A. Ureña, A. Piarristeguy, A. Pradel, and M. Fontana, Appl. Surf. Sci. **254** (2007) 321.
24. A. Piarristeguy, M. Ramonda, A. Ureña, A. Pradel, and M. Ribes, J. Non-Cryst. Solids **353** (2007) 1261.
25. A. Piarristeguy, M. Ramonda, N. Frolet, M. Ribes, and A. Pradel, Solid State Ionics **181** (2010) 1205.
26. L. Rátkai, I. Kaban, T. Wágner, J. Kolář, S. Valková, I. Voleská, B. Beuneu, and P. Jóvári, J. Phys.-Condens. Mat. **25** (2013) 454210.